PAPER

Check for updates

Magnetic ordering of the cryogenic magnetic cooling mineral gaudefroyite†

Rukang Li,[*ab] Pascal Manuel,[c] Fabio Orlandi [ID][c] and Colin Greaves [ID][*d]

The mineral gaudefroyite, $Ca_4Mn_3O_3(BO_3)_3CO_3$, contains chains of edge-linked MnO_6 octahedra such that the Mn^{3+} ions are located on a Kagomé lattice (perpendicular to the chains), which frustrates antiferromagnetic order. In the temperature range 6–24 K, small changes in magnetic field cause large entropy changes and give excellent magnetocaloric properties. Neutron powder diffraction data have therefore been collected in various magnetic fields over this temperature range to reveal the nature of the low temperature structural and magnetic properties. At temperatures below 10.2(1) K, the magnetic moments on the Mn^{3+} ions (3.28(5) μ_B at 100 mK) order to give a typical Kagomé antiferromagnetic $q = 0$ structure, according to a 2-dimensional XY scaling law. The magnetic frustration causes the magnetic order to be very sensitive to applied magnetic fields: a field of only 1 T rotates the moments such that 90% of the overall moment corresponds to ferromagnetic order. The properties are discussed in relation to the exceptional low field magnetocaloric properties of this mineral.

Introduction

Gaudefroyite, a mineral with the composition $Ca_4Mn_3O_3(BO_3)_3CO_3$, was first discovered in Morroco by J. F. Gaudefroy, after whom it was named.[1] The most important structural feature is the presence of linear, parallel chains of edge-shared MnO_6 octahedra connected by BO_3 groups. The hexagonal structure, space group $P6_3/m$, is shown in Fig. 1(a) where the chains run parallel to c and form a typical Kagomé net in the ab plane (Fig. 1(b)).[2] Ca^{2+} ions and CO_3 groups occupy the tunnels formed between the chains and the BO_3 linkage groups (Fig. 1(c)). The Mn^{3+} (d^4) ions are in an elongated octahedral environment with the long bonds being to the linking O atoms. These bonds (2.286(7) Å) are marked in green in Fig. 1(b) and the shorter bonds (1.873(4) Å) are marked in magenta. Each linking O atom therefore forms two bonds to adjacent Mn ions *via* either two half-occupied Mn d_{z^2} orbitals or two empty Mn $d_{x^2-y^2}$ orbitals. All strong intrachain magnetic exchange occurs through $\sim90°$ Mn–O–Mn super-exchange paths favouring ferromagnetic (FM) order. Magnetic measurements[3] confirmed the predominant FM coupling of Mn^{3+} ions along each chain with Weiss constant $\theta = +45$ K,

while frustration exists between the chains and was originally thought to result in a freezing temperature of approximately 10 K. At sufficiently low temperatures, the FM MnO_6 chains have been considered as "giant spins" located on a Kagomé lattice.[3]

The magnetocaloric effect (MCE) is an important phenomenon which is vital for achieving extremely low temperatures and is based on the large temperature decrease that can occur when the magnetic field applied to a magnetic material is removed under adiabatic conditions. The effect is determined by the magnetic entropy change that is associated with the change in field. Theoretically, it has been predicted that geometrically frustrated spin systems associated with Kagomé, garnet and pyrochlore lattices could produce strongly enhanced MCE, and also a rapid cooling rate, resulting from the large entropy attributed to the highly degenerate magnetic ground states in zero field.[4–6] Gaudefroyite therefore seems to fulfil all the requirements as a practical MCE material to operate in the cryogenic temperature range.

In a previous report,[7] we demonstrated that gaudefroyite does indeed have unique low temperature MC properties in relatively low magnetic fields, and is subject to very rapid cooling rates. For example, Fig. 2 shows the entropy change for a field of 2 T and compares it with that for an excellent Gd MCE material, $Gd(HCOO)_3$.[8] At this field, the entropy change peaks at 7 J kg^{-1} K^{-1} for a temperature of 12 K, but is higher than that for the Gd salt at all temperatures above 9 K, and substantially so at 20 K, the boiling point of hydrogen. The inset to Fig. 2, reproduced from ref. 7, shows the response time (60 ms) to a cyclical change in field from 0 to 750 mT at 15 K. These excellent low field properties could be very usefully applied for liquefying

aBeijing Centre for Crystal Research and Development, Key Laboratory of Functional Crystals and Laser Technology, Technical Institute of Physics and Chemistry, Chinese Academy of Sciences, Beijing 100190, P. R. China. E-mail: rkli@mail.ipc.ac.cn

bUniversity of Chinese Academy of Sciences, Beijing 100049, P. R. China

cISIS Facility, STFC Rutherford Appleton Laboratory, Didcot OX11 0QX, UK

dSchool of Chemistry, University of Birmingham, Birmingham B15 2TT, UK. E-mail: c.greaves@bham.ac.uk

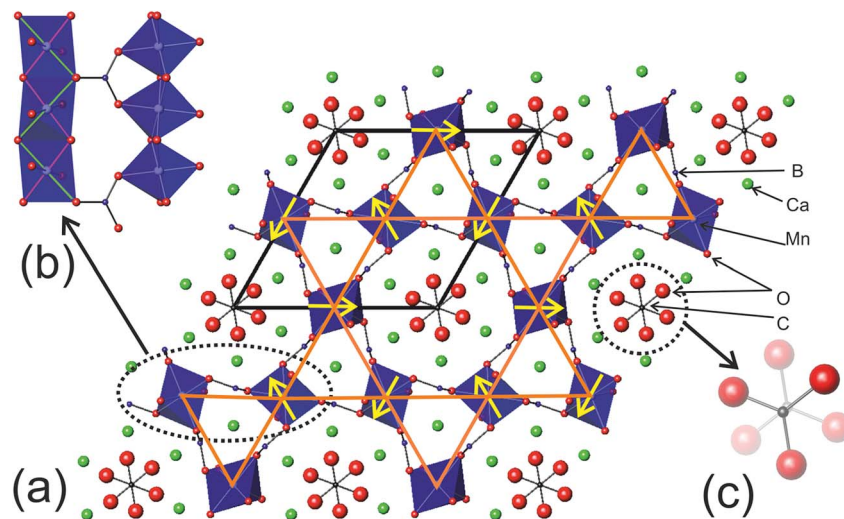† Electronic supplementary information (ESI) available. See DOI: 10.1039/c8ta08851a

This journal is © The Royal Society of Chemistry 2018

J. Mater. Chem. A, 2018, **6**, 21149–21155 | 21149

Fig. 1 (a) The crystal structure of gaudefroyite viewed along [001]. The unit cell is shown (black line) and the Kagomé lattice (orange line) defined by the coplanar Mn ions. The yellow arrows show the directions of the Mn magnetic moments in the $q = 0$ magnetic structure found in the Y-substituted gaudefroyite.[14] (b) Chains of edge-linked MnO_6 octahedra along [001] connected by B atoms which form planar BO_3 (borate) groups. See text for the bonds marked in green or magenta. (c) Channels formed between the chains contain Ca ions and CO_3 groups. The CO_3 groups are disordered and occupy closely spaced antisymmetric positions with 50% occupancy, as shown.
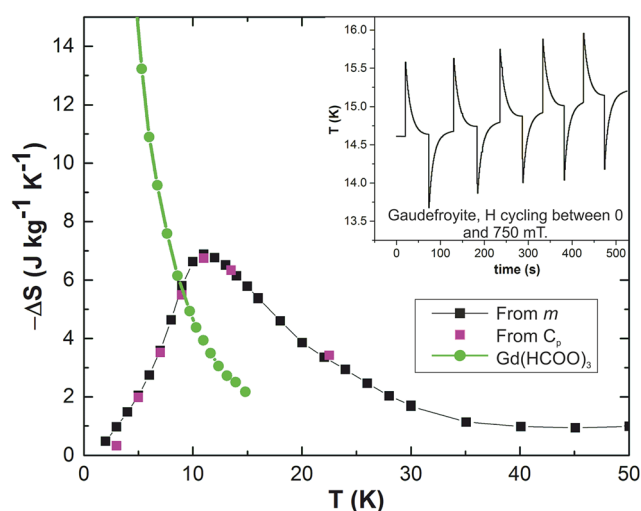

Fig. 2 Entropy changes of gaudefroyite for a field of 2 T obtained from the magnetisation (m in legend) and specific heat (C_p in legend) measurements; the data are compared with those for $Gd(HCOO)_3$.[8] Inset: temperature change of gaudefroyite on cycling between fields of 0 and 750 mT.

hydrogen, for storage or transport, in an energy framework that includes hydrogen. Other potential candidates for this application have serious problems. Paramagnetic Gd salts are very effective at low temperatures but are inefficient at 20 K as shown in Fig. 2. On the other hand, Gd alloys have excellent characteristics near ambient temperatures but their efficiencies decrease rapidly on cooling and are comparable with gaudefroyite at 20 K. However, the alloy materials show limited stability in liquid hydrogen.[9] Gaudefroyite, being an oxide, is unique in being stable in hydrogen and having excellent properties at 20 K. Moreover, it satisfies another requirement in that

it contains no expensive rare earth elements. The MCE properties of gaudefroyite are therefore of great importance, and a detailed study of the mineral's low temperature magnetic properties is essential to understand the origin of the MCE behaviour.

The properties, of course, are clearly determined by the behaviour of the magnetic moments on the Mn^{3+} ions, but the expected behaviour of such magnetic frustration on a Kagomé lattice is not clear and has been the focus of many discussions. It has been shown theoretically[10] that, in an ideal situation at a finite temperature, there should be no long-range magnetic order for the spins on a Kagomé lattice. Subsequently, however, transitions to ordered states in Kagomé systems were observed and various mechanisms – order introduced by disorder, by anisotropy, by next–next neighbour *etc.* – were proposed.[11–13] Such interactions may result in one of two antiferromagnetic (AFM) magnetic structures, commonly labelled $\sqrt{3} \times \sqrt{3}$ type order and $q = 0$, 120° order as discussed, for example, in ref. 14. Previously, we observed that the Y-substituted gaudefroyite, $YCa_3Mn_3O_3(BO_3)_4$, ordered into a typical $q = 0$ state below 9 K (Fig. 1),[15] and the disordered Y/Ca sites were proposed as a possible origin for the magnetic order. In contrast, the Ca-sites are fully ordered in gaudefroyite and the magnetisation data showed no convincing evidence of such a phase transition.

The low temperature magnetic state of gaudefroyite is fundamentally important, not only as a basis for our understanding of its unique MCE behaviour, but also more widely for discussions of the statistical properties of frustrated Kagomé systems. Although the crystal structure of gaudefroyite from single crystal X-ray diffraction studies has been reported,[2,16–18] its magnetic structure has never been determined *via* neutron diffraction because the natural B in the mineral is highly absorbing. Unfortunately, ^{11}B-enriched synthetic gaudefroyite is not available using conventional solid state methods because

21150 | *J. Mater. Chem. A*, 2018, **6**, 21149–21155

This journal is © The Royal Society of Chemistry 2018

of the thermal loss of the carbonate group. Here we report a neutron powder diffraction (NPD) study of the natural mineral which demonstrates that high quality data are possible for such B-containing samples using high intensity sources. Data, collected from the mineral at various temperatures and magnetic fields, have revealed for the first time that gaudefroyite does, in fact, order magnetically; our results therefore provide the critical basis for discussions concerning the origin of its excellent MCE properties in the temperature range 6–24 K.

Experimental

The mineral sample used in the present (NPD) study was obtained as aggregates of single crystals (several mm in all directions) from the same origin as the previous report,[7] Wessels Mine, Kalahari Manganese Field, Northern Cape Province, South Africa. The crystals were contaminated with a very small amount of a red powder, which was identified as the garnet andradite, $Ca_3Fe_2(SiO_4)_3$, by single crystal X-ray diffraction. After removal of the majority of this contaminant, the gaudefroyite crystals were crushed to a fine powder and XRF analysis revealed no significant impurities; traces of Fe and Si (1% and 0.6% by weight, respectively), were attributed to residual andradite.

To avoid movement of the gaudefroyite grains in applied magnetic fields, the powdered sample was pressed into nine pellets, each of 5 mm diameter. The pellets (total mass 2.06 g) were stacked to provide a total length of 3.6 cm, placed into a 6 mm diameter copper can and tightly fixed in place with a Cd rod. The copper can was chosen to ensure good thermal conduction. NPD data were collected on the instrument WISH at ISIS, STFC Rutherford Appleton Laboratory.[19] Cryogenic temperatures as low as 100 mK were achieved in a cryomagnet with a dilution refrigerator insert. Data were collected in the temperature range from 100 mK to 15 K at about 1 K intervals in zero field, and for the temperatures 100 mK, 5 K, 11 K and 15 K, in fields from 0 T to 3 T.

Rietveld refinements against the collected NPD patterns were carried out using the GSAS package.[20] In order to take full advantage of the high resolution and wide range of d values (including the main magnetic peak), joint refinements were performed on patterns collected by the detector banks with average $2\theta = 58.33°$ and $121.66°$. The absorption coefficient (μ_R) of the sample (predominantly from B and Mn) was determined from standard absorption cross sections of the elements[21] with the following equation:

$$\mu_R = \frac{\sigma \times N \times \rho \times R}{M}$$

where σ is the sum of all the absorption cross sections at 1.0 Å for all the atoms in the formula unit (434.2×10^{-24} cm^2), N is the Avogadro number, ρ is the estimated sample density (2.91 g cm^{-3}), R is the sample radius and M is the molecular mass (609.5 g). This yields $\mu_R = 0.94$, which was adopted and fixed at this value for all refinements.

Because of the anisotropic crystal morphology, some preferred orientation of the crystallites was apparent and was

modelled using the March–Dollase correction. Since the magnetic parameters were correlated with the preferred orientation parameter, the preferred orientation of the sample was initially determined from the non-magnetic, 15 K, dataset; this correction was then applied to all datasets for the magnetic refinements. Since a copper can was used for sample containment, all the diffraction patterns contain strong reflections from the Cu metal for $d < 2.1$ Å. Due to the complex nature of the texture of the Cu metal can, the peaks can be modelled only by le Bail extraction[22] with a dummy atom at the origin. Only the global parameters–lattice parameters and peak profile parameters – were refined for the Cu can.

Results and discussion

Typical neutron diffraction patterns of the lower resolution banks ($2\theta = 58.33°$) are shown in Fig. 3. After lowering the temperature, an intense magnetic diffraction peak appears and can be assigned to the 100 reflection; other, weaker peaks are also commensurate with the nuclear unit cell as shown by the difference plot of 3–15 K patterns (Fig. 3). The magnetic diffraction peaks are inconsistent with the $\sqrt{3} \times \sqrt{3}$ type order, but strongly support $q = 0$ order,[23–25] which was also observed in the Y-substituted gaudefroyite and is shown in Fig. 1(b).[15] The observation of magnetic order in gaudefroyite was a little surprising since we previously attributed the order in the substituted phase to Ca/Y disorder, which is absent in the parent gaudefroyite. Joint refinements on both lower and high resolution banks ($2\theta = 58.33°$ and $121.66°$, respectively) with the magnetic model of Fig. 1(b) were therefore performed for all the patterns collected from 100 mK to 15 K. Notwithstanding the very large Cu peaks from the can, good refinements based on all datasets were achieved, with typical refined patterns shown in ESI, Fig. S1†. For the nuclear structure, two models,
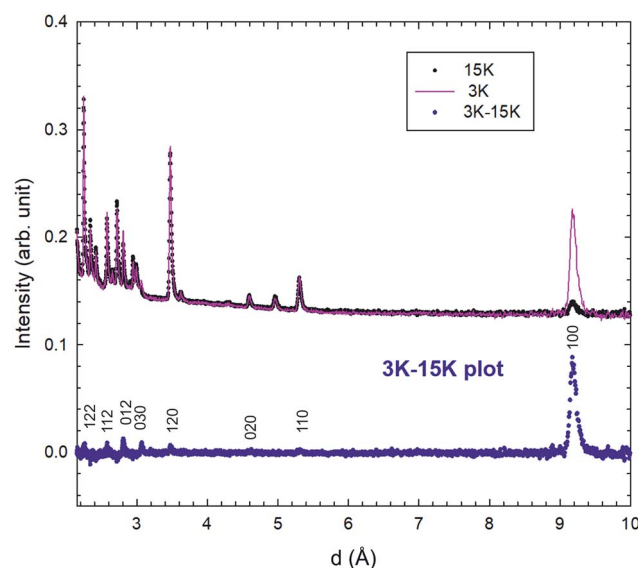

Fig. 3 Neutron powder diffraction patterns of gaudefroyite at 15 K (above the AFM transition) and 3 K (AFM ordered); the curve with blue dots at lower part is the difference plot of the 3–15 K data.

This journal is © The Royal Society of Chemistry 2018

J. Mater. Chem. A, 2018, **6**, 21149–21155 | **21151**

with space groups of $P6_3$ and $P6_3/m$, were examined based on previous reports of single crystal X-ray diffraction studies of mineral samples from different origins.[16–18] The higher symmetry space group, $P6_3/m$, was found to be more stable and was therefore adopted for the nuclear structure throughout this study; the magnetic structure corresponds to the Shubnikov magnetic space group $P6_3'/m'$. We also arbitrarily aligned one of the magnetic moments (for Mn^{3+} at (0.5,0,0)) to point along the a-axis (m_x in Table S1†), since powder diffraction prevents location of the direction of the moments in the ab plane for nuclear hexagonal symmetry.

Evidence for ordering of the moments on the Mn^{3+} ions was first observed below 11 K and reached a moment of 3.28(5) μ_B at 100 mK, which is only 82.5% of the ideal, spin-only, ordered moment of 4 μ_B for Mn^{3+} (d^4, high spin). Although a reduction is expected because of covalence in the Mn–O bonds, geometric frustration may cause further reduction as observed in other systems like jarosites.[25] In addition, the refinements allow a small degree of AFM tilting of the moments out of the ab plane, which could also contribute to the reduction. The variation of magnetic moment with temperature was explored and found to fit a 2-d scaling law (see Fig. S2†) except for small moments close to T_N, where correlation effects between nuclear and magnetic parameters resulted in slightly unreliable data. The magnetic contribution to the 100 reflection, the most intense magnetic peak, was therefore also used to monitor the temperature evolution as shown in Fig. 4(a). After subtraction of the small nuclear contribution (I_N), the variation of integrated magnetic intensity (I) with temperature was found (see Fig. 4(b)) to obey the scaling law:[26]

$$I - I_N = I_0\left(1 - \frac{T}{T_N}\right)^{2\beta}$$

with $T_N = 10.2(1)$ K and $\beta = 0.20(2)$. Since the magnetic scattering intensity (I) is proportional to the square of the magnetic moment, we adopt an exponent of 2β to allow direct comparison with the data from the variation of the moment (Fig. S2†). The exponent parameter, β, is in accordance with the 2-d XY model[26] and is consistent with the moment being within the ab plane. The small decrease in magnetic intensity below 3 K may imply

possible enhancement of frustration below this temperature but could also relate to other fluctuation mechanisms.

We previously reported that gaudefroyite has exceptional MCE properties especially at low fields around 10 K, with $\Delta S > 3$ J kg^{-1} K^{-1} at a field change of 2 T over the full temperature range 6–24 K, see Fig. 2(a).[7] However, our NPD data clearly show that gaudefroyite displays AFM order below 10.2 K which, in principle, might be expected to allow only limited MCE properties below this temperature because the magnetic entropy is normally frozen out in ordered states. Early magnetization measurements on single crystals of gaudefroyite[3] also showed that the moment is highly susceptible to applied magnetic fields, both parallel and perpendicular to the ab plane: an applied field of 0.5 T produces a magnetization amounting to 60% of its saturated value, a behaviour similar to a ferromagnet.[27] Since these factors seem incompatible with the AFM ordered state determined by the NPD data, the magnetic properties in applied magnetic fields were examined by collecting NPD patterns at 100 mK in fields of up to 3 T in steps of 0.5 T.

The application of a magnetic field changed the magnetic diffraction peaks drastically as shown in Fig. 5(a). At 3 T, the AFM peaks are seen to have disappeared and are replaced by magnetic scattering that increases the intensity of selected nuclear peaks. It was found that two magnetic phases were needed to refine the NPD patterns: the $q = 0$ triangular AFM ordered phase along with a FM phase with moments m_x and m_z along the x and z directions, respectively. The x-axis in the ab plane was arbitrarily chosen since the uniaxial symmetry of gaudefroyite renders NPD unable to determine the direction of the component which lies perpendicular to the z-axis. The total FM moment corresponds to $m_{FM} = (m_x^2 + m_z^2)^{1/2}$. The observed and calculated profiles show good agreement (Fig. S3†) and the refined moments are shown in Fig. 5(b).

The refinements demonstrate that the FM components along x and z directions are equal within experimental error and grow continuously as the field increases, at the expense of the AFM phase. At ~0.75 T, both ferromagnetic components are larger than the AFM moment, and at 1 T the FM components comprise ~90% of the total Mn moment. These findings
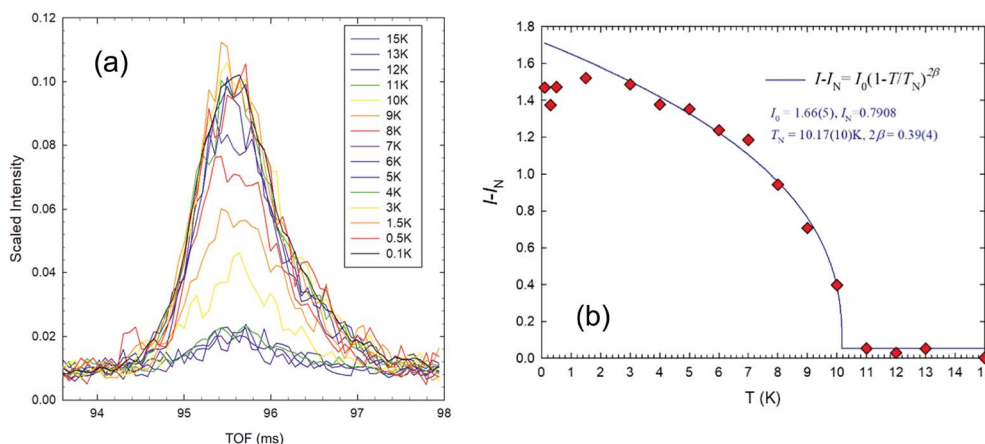

Fig. 4 (a) Plots of intensity against time of flight (TOF) for the magnetic 100 peaks and (b) integrated intensities of the 100 magnetic peaks for gaudefroyite at temperatures from 100 mK to 15 K.
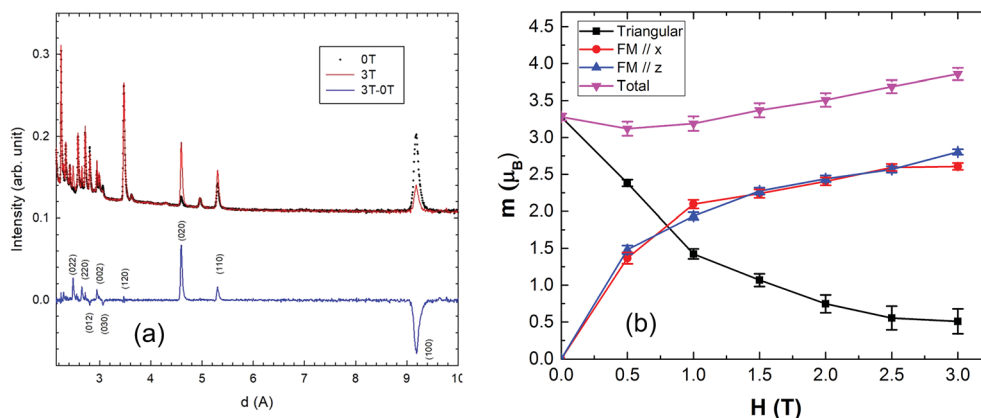
21152 | J. Mater. Chem. A, 2018, 6, 21149–21155

This journal is © The Royal Society of Chemistry 2018

Fig. 5 (a) NPD patterns of gaudefroyite under fields of 0 T and 3 T at 100 mK and the difference profile showing the scattering from the FM order; (b) variation of the refined ordered magnetic moments with magnetic field.

underline the observation that the moment is highly sensitive to applied magnetic fields and provides the origin of the excellent MCE properties at low fields,[3,7] despite the fact that gaudefroyite is actually antiferromagnetically ordered below 10.2 K.

For NPD refinements against data collected in a magnetic field, the Mn magnetic moment components m_x and m_z were always found to be equal within experimental error. This can be seen, for example, in the refinements for data collected at 100 mK in fields from 0.5 T to 3 T, shown in Fig. 5(b). Magnetic measurements show that the material is virtually saturated at 3 T,[3] so the magnetic moments in each crystallite are certainly aligned in the field direction at this field. Given that for a powder sample we can determine only m_x and m_z because of the symmetry, the orientation of the experimental moment, 45° to z, relates to averaging effects caused by the random distribution of crystals with respect to the applied field. Since the orientation does not vary with field, we assume that the FM moment is approximately in the direction of the field for all fields applied. However, the individual m_x and m_z vectors have no special significance and only their sum, m_{FM} is important. Nevertheless, additional support for the averaging explanation is provided by refinement against data collected at 15 K, *i.e.* significantly above T_N, in a field of 3 T (*vide infra*).

Fig. S4(a)† shows the effect of the 3 T magnetic field on the NPD data at 15 K, for which the FM moment is expected to be oriented exactly in the field direction. A large FM degree of order occurred giving NPD profiles that were almost identical to those obtained in this field at lower temperatures. Structure refinement, Fig. S4(b),† again resulted in equal moments along x and z ($m_x = 2.18(7)$ μ_B, $m_z = 2.06(6)$ μ_B), consistent with the orientation of m_{FM} being primarily determined by the crystallite distribution. The combined moment, 2.99(9) μ_B, shows that 75% magnetic saturation occurs even at a temperature 5 K above T_N and is consistent with the excellent MCE properties in the paramagnetic region. NPD datasets in 3 T at 5 K and 11 K were also analysed. The direction of the FM moments was unchanged and the variation in moment magnitude is plotted in Fig. 6. It is very interesting that the FM moment induced by the magnetic field decreases regularly as the temperature

increases, which would be expected for a simple FM material, and illustrates that the frustrated AFM order has little hindrance to the moment rotation to give FM ordering in a magnetic field; this is important for the provision of good MCE behaviour below T_N.

The energy scale of the Néel temperature ($T_N = 10.2(1)$ K) of gaudefroyite, 85 J mol^{-1}, corresponds to the magnetic energy ($\mu_B H$) for a field of $H = 15$ T, about 20 times more than the observed field needed to destroy the AFM order. The origin of the enhanced flexibility with the applied field must come from the FM chain along c and the frustration from the Kagomé lattice in the ab plane. Taking into consideration the previous magnetisation studies,[3] the present system may be represented by the following Hamiltonian:

$$\mathscr{H} = -2J_c S_i S_{i+c} + 4J_{ab} S_i S_{i+ab} + D(S_i^z)^2$$

where J_c, J_{ab} are the intrachain and interchain exchange strengths and D is the single-ion anisotropy. Previously, $J_c = 4.2$
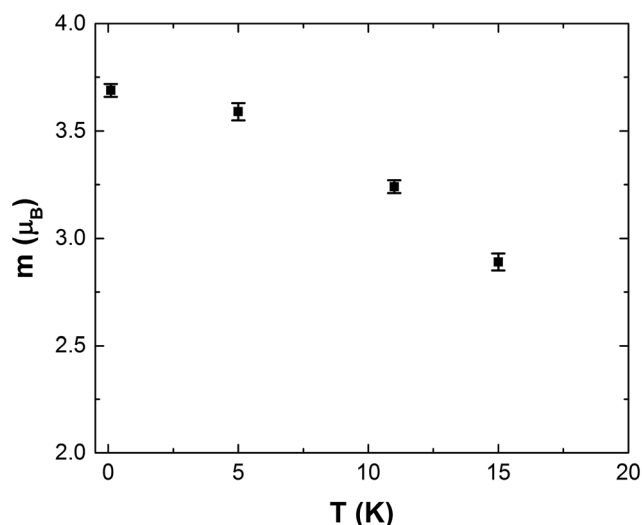

Fig. 6 Variation in magnetic moment with temperature for the FM ordered gaudefroyite in a field of 3 T.

This journal is © The Royal Society of Chemistry 2018

J. Mater. Chem. A, 2018, **6**, 21149–21155 | **21153**

K and $D = 0.67$ K have been obtained from fitting the susceptibilities along ab and c directions, respectively.[3] J_{ab} can be estimated from second order Green's function theory and the relation:[28]

$$T_N = 4S(S+1)\sqrt{J_c J_{ab}}$$

With $T_N = 10.2$ K and $S = 2$ (Mn^{3+}, high spin), the interchain interaction can be obtained as $J_{ab} = 0.043$ K, which is a rather small energy arising from the super-super-exchange through Mn–O–B–O–Mn or dipole–dipole interactions and depressed by the in-plane frustration. Since J_{ab} corresponds to a magnetic energy associated with a field of only ∼60 mT, the high sensitivity of magnetic order and magnetisation to small fields is explained. It is clear that the intrachain FM exchange is the dominant magnetic interaction and results in what may be envisaged as a condensed single chain magnet,[29] and the relatively high ordering temperature is enhanced by the large intrachain interactions. Nevertheless, it must be pointed out that J_{ab} is only a nominal value because the in-plane frustration is included, which usually tends to lower the ordering temperature. It is well known that the Kagomé lattice provides a high level of frustration, hence J_{ab} obtained here might underestimate the actual exchange by a factor of 10.[30]

It is important to consider fully the results of this study in relation to the MCE properties of gaudefroyite. In this way we may be able to signpost better low temperature materials, or materials that can be applied for adiabatic cooling at higher temperatures. Fig. 2 shows that gaudefroyite undergoes a high magnetic entropy change as a magnetic field is applied or removed, and this occurs both above and below the magnetic ordering temperature. Above T_N, we have shown that magnetic fields can induce large FM moments which will result in a decrease in entropy and provide the MCE effect. Indeed, the inset to Fig. 2 shows the effect at 15 K in the small field of 750 mT. However, for this simple mechanism, large entropy changes (and correspondingly excellent MCE properties) require large fields even for large magnetic moments, such as those for Gd^{3+} ions ($S = 7/2$). Fig. 2 shows that in this paramagnetic region, $-\Delta S$ is ∼3 times larger for gaudefroyite than $Gd(HCOO)_3$. These observations confirm the presence of FM clusters that act as "giant" moments in gaudefroyite near T_N. In fact, magnetisation data suggest that anisotropy associated with cluster formation occurs at significantly higher temperatures (certainly at 20 K) and the Curie–Weiss law is not obeyed. Although the entropy change decreases quite rapidly below T_N, Fig. 2 shows that there is no discontinuity that we might expect for a transition to a magnetically ordered state with very small magnetic entropy. Some level of disorder remains which could originate from simple frustration and also from the inherent entropy that is present in magnetically ordered Kagomé lattices. Given that this disorder is likely to extend within each chain that forms a giant moment, these effects are likely to be substantial. We therefore see that the excellent MCE properties of gaudefroyite, which extend over a wide temperature range, are the result of a co-operative effect involving the inherent frustration of the Kagomé lattice of Mn^{3+} ions together with the formation of chains of FM coupled Mn^{3+} ions to provide giant moments – and therefore a very large entropy increase – when a small magnetic field is removed. The magnetic frustration, with very small interchain magnetic exchange, explains the observation of the high MCE below the magnetic ordering temperature and also results in the exceptionally rapid temperature change as seen in Fig. 2. Our results highlight the need to examine related phases that contain similar structural and magnetic features. In particular, we need chains of edge-linked octahedrally coordinated ions with strong 90° M–O–M FM exchange interactions at both linking O atoms; the chains need to be magnetically frustrated in the plane perpendicular to the chains. The electronic properties of Cr^{3+} (d^3), Fe^{3+} (d^5) and Jahn–Teller distorted Mn^{3+} (d^4) ions offer most promise.

Conclusions

The mineral gaudefroyite orders magnetically to give a typical $q = 0$ Kagomé antiferromagnetic state with a Néel temperature of $T_N = 10.2(1)$ K. The ordered moment on the Mn^{3+} ion follows a scaling law with $\beta = 0.20(2)$, in accordance with a 2-dimensional XY spin system. Due to the large ratio of the strong intrachain FM interaction, $J_c = 4.2$ K, compared to that between the chains, $J_{ab} = 0.043$ K, the ordered AFM state can easily be destroyed with a small applied magnetic field, e.g. at 100 mK a field of 1 T aligns 90% of the overall moment to the field direction. This high flexibility with field change and the corresponding high entropy change, result from the formation of single chain giant magnets and is the origin of the excellent MCE properties. Although synthesis of gaudefroyite is problematic, it is important to note that substituted analogues are possible as previously reported.[7,15] Indeed, $GdCa_3Mn_3O_3(BO_3)_4$ has even better low temperature MC properties than gaudefroyite itself.[7]

Conflicts of interest

There are no conflicts of interest to declare.

Acknowledgements

References

1 G. Jouravsky and F. Permingeat, *Bull. Soc. Fr. Mineral. Cristallogr.*, 1964, **87**, 216–219.
2 M. M. Granger and J. Protas, *C. R. Acad. Sci.*, 1965, **260**, 4553–4555.

3 R. K. Li and C. Greaves, *Phys. Rev. B: Condens. Matter Mater. Phys.*, 2004, **70**, 132411.

4 M. E. Zhitomirsky, *Phys. Rev. B: Condens. Matter Mater. Phys.*, 2003, **67**, 104421.

5 J. Schnack, R. Schmidt and J. Richter, *Phys. Rev. B: Condens. Matter Mater. Phys.*, 2007, **76**, 054413.

6 S. S. Sosin, L. A. Prozorova, A. I. Smirnov, A. I. Golov, I. B. Berkutov, O. A. Petrenko, G. Balakrishnan and M. E. Zhitomirsky, *Phys. Rev. B: Condens. Matter Mater. Phys.*, 2005, **71**, 094413.

7 R. K. Li, G. J. Li and C. Greaves, *J. Mater. Chem. A*, 2018, **6**, 5260–5264.

8 G. Lorusso, J. W. Sharples, E. Palacios, O. Roubeau, E. K. Brechin, R. Sessoli, A. Rossin, F. Tuna, E. J. L. McInnes, D. Collison and M. Evangelisti, *Adv. Mater.*, 2013, **25**, 4653–4656.

9 T. Numazawa, K. Kamiya, T. Utaki and K. Matsumoto, *Cryogenics*, 2014, **62**, 185–192.

10 D. A. Huse and A. D. Rutenberg, *Phys. Rev. B: Condens. Matter Mater. Phys.*, 1992, **45**, 7536–7539.

11 J. N. Reimers and A. J. Berlinsky, *Phys. Rev. B: Condens. Matter Mater. Phys.*, 1993, **48**, 9539–9554.

12 A. L. Chernyshev and M. E. Zhitomirsky, *Phys. Rev. Lett.*, 2014, **113**, 237202.

13 A. B. Harris, C. Kallin and A. J. Berlinsky, *Phys. Rev. B: Condens. Matter Mater. Phys.*, 1992, **45**, 2899–2919.

14 M. Nishiyama, S. Maegawa, T. Inami and Y. Oka, *Phys. Rev. B: Condens. Matter Mater. Phys.*, 2003, **67**, 224435.

15 R. K. Li and C. Greaves, *Phys. Rev. B: Condens. Matter Mater. Phys.*, 2003, **68**, 172403.

16 O. V. Yakubovich, M. A. Simonov and N. V. Belov, *Crystallogr. Rep.*, 1975, **20**, 152–155.

17 C. Hoffmann, T. Armbruster and M. Kunz, *Eur. J. Mineral.*, 1997, **9**, 7–19.

18 S. M. Antao and I. Hassan, *Can. Mineral.*, 2008, **46**, 183–193.

19 L. C. Chapon, P. Manuel, P. G. Radaelli, C. Benson, L. Perrott, S. Ansell, N. J. Rhodes, D. Raspino, D. Duxbury, E. Spill and J. Norris, *Neutron News*, 2011, **22**, 22–25.

20 A. C. Larson and R. B. von Dreele, *General Structure Analysis System*, Los Alamos National Laboratory, Los Alamos, NM, USA, 1994.

21 V. F. Sears, *Neutron News*, 1992, **3**, 26–37.

22 A. Le Bail, *Powder Diffr.*, 2005, **20**, 316–326.

23 A. L. Chernyshev and M. E. Zhitomirsky, *Phys. Rev. B: Condens. Matter Mater. Phys.*, 2015, **92**, 144415.

24 O. Goetze and J. Richter, *Phys. Rev. B: Condens. Matter Mater. Phys.*, 2015, **91**, 104402.

25 A. S. Wills, A. Harrison, C. Ritter and R. I. Smith, *Phys. Rev. B: Condens. Matter Mater. Phys.*, 2000, **61**, 6156–6169.

26 A. Taroni, S. T. Bramwell and P. C. W. Holdsworth, *J. Phys.: Condens. Matter*, 2008, **20**, 275233.

27 H. Park, R. Lam, J. E. Greedan and J. Barbier, *Chem. Mater.*, 2003, **15**, 1703–1712.

28 P. M. Richard, *Phys. Rev. B: Solid State*, 1974, **10**, 4687–4689.

29 C. Coulon, H. Miyasaka and R. Clérac, *Struct. Bonding*, 2006, **122**, 163–206.

30 J. E. Greedan, *J. Mater. Chem.*, 2001, **11**, 37–53.

This journal is © The Royal Society of Chemistry 2018

J. Mater. Chem. A, 2018, **6**, 21149–21155 | **21155**